

Review

A Review on Catalytic Nanomaterials for Volatile Organic Compounds VOC Removal and Their Applications for Healthy Buildings

Kwok Wei Shah ^{*,†}  and Wenxin Li [†]

Department of Building, School of Design and Environment, National University of Singapore, 4 Architecture Drive, Singapore 117566, Singapore; bdglw@nus.edu.sg

* Correspondence: bdgskw@nus.edu.sg

† These authors contributed equally to this work.

Received: 5 May 2019; Accepted: 19 June 2019; Published: 23 June 2019



Abstract: In order to improve the indoor air quality, volatile organic compounds (VOCs) can be removed via an efficient approach by using catalysts. This review proposed a comprehensive summary of various nanomaterials for thermal/photo-catalytic removal of VOCs. These representative materials are mainly categorized as carbon-based and metallic oxides materials, and their morphologies, synthesis techniques, and performances have been explained in detail. To improve the indoor and outdoor air quality, the catalytic nanomaterials can be utilized for emerging building applications such as VOC-reduction coatings, paints, air filters, and construction materials. Due to the characteristics of low cost, non-toxic and high chemical stability, metallic oxides such as TiO₂ and ZnO have been widely investigated for decades and dominate the application market of VOC-removal catalyst in buildings. Since other catalysts also showed brilliant performance and have been theoretically researched, they can be potential candidates for applications in future healthy buildings. This review will contribute to further knowledge and greater potential applications of promising VOC-reducing catalytic nanomaterials on healthier buildings for a better indoor and outdoor environment well-being.

Keywords: nanomaterials; VOCs removal; photocatalysis; thermal oxidation; catalytic oxidation; healthy buildings; green application; photocatalytic reactor

1. Introduction

Healthy buildings aim to provide a healthy built environment for occupants inside buildings, and indoor air quality can significantly impact occupants' health [1]. Since people spend most of their time inside buildings, indoor air quality has become an increasing concern. Indoor air quality can be affected by various factors including toxicological, microbiological, physical systems, indoor, and outdoor ventilations [2]. The advances in construction technology have produced numerous applications of synthetic building materials, but have also brought some adverse effects on the indoor environment, including the major pollution from volatile organic compounds (VOCs). VOCs are defined as having a boiling point that ranges between 50 °C and 260 °C [3]. They can contribute to the formation of ozone and fine particulates in the atmosphere [4] and work directly as toxic substances to the environment and human being. The exposure to VOCs can result in both acute and chronic health effects including respiratory diseases, impaired neurobehavioral function, and sick building syndrome, etc. [2].

In order to remove the VOCs, many methods have been proposed and can be roughly divided into two main groups according to their mechanisms: adsorption techniques and oxidation techniques [5], or the combination of them [6]. The former one is a conventional method by transferring VOCs from the air to the solid phase via adsorbents, e.g., activated carbon [7], biochar [8] and fibre [9], etc. which

faces challenges like saturation and pore blockages. The latter oxidation techniques provide a better approach to cost-effectively remove VOCs, which show higher degradation activity towards polar VOCs (OVOCs > Ahs > AIHs) [10]. Photo and thermal catalytic oxidation are two of the most common oxidation techniques. Thermal oxidation reactions require a high temperature above 600 °C, and the oxidation efficiency grows with the temperature increase. The technique of photocatalytic oxidation commonly uses nano-semiconductor catalysts and ultraviolet (UV) light to convert organic compounds in indoor air into benign and odourless constituents—water vapor (H₂O) and carbon dioxide (CO₂) for air purification [5,11,12]. Figure 1 shows the basic principle of photocatalytic oxidation for the removal of VOCs. An electron in an electron-filled valence band (VB) is excited by photoirradiation to a vacant conduction band (CB), leaving a positive hole in the VB. Later, the photogenerated electrons and holes can react with H₂O and O₂ molecules to reduce and oxidate VOCs on the surface of a photocatalyst [12–14].

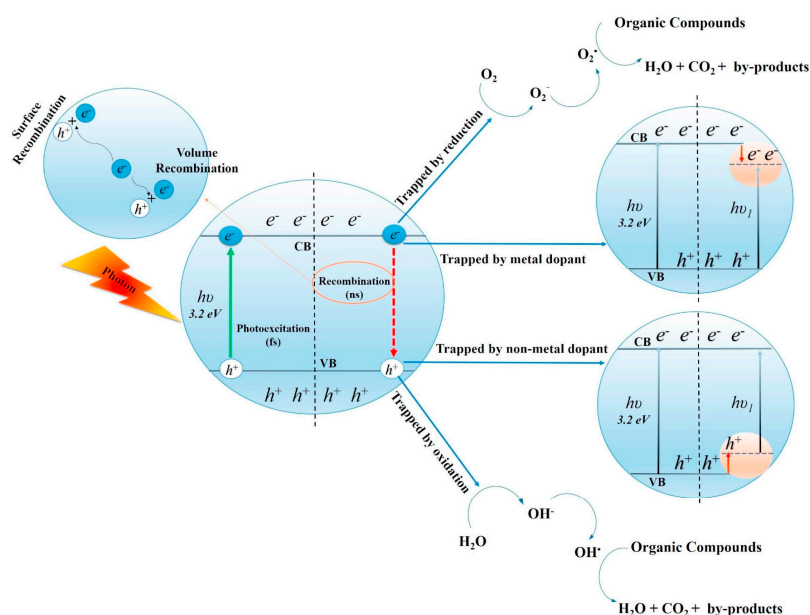


Figure 1. Mechanisms of photocatalytic oxidation for the removal of VOCs [14]. (reproduced from [14], with permission from Elsevier, 2019).

Most of the VOCs in indoor air are aromatics, aldehydes, and halocarbons, and they are rich in the established, new and renovated buildings [15]. Measurements indicate that similar exposure level is shared by VOCs in various indoor and building materials, and coverings are the major sources of VOCs [16]. VOCs are common in industry [5] and widely used in construction projects. Since many VOCs will off-gas a significant proportion of their volume in a relatively short time, the VOC concentrations could be much higher than typical ambient levels in newly-constructed or decorated buildings [2]. To reduce the VOC emissions and indoor concentrations inside the buildings, some proposed to bake-out the housing unit with a radiant floor-heating system [17], and a long-enough bake-out could deplete solvents and reduce VOC emissions [18]. While a more efficient method is to adopt photocatalysis such as TiO₂, these materials can be applied on buildings as a coating or paint, or synthesised with mortar, which will further affect the aesthetics, sanitation and efficiency of the buildings [19–21]. Therefore, special attention should be paid to the construction materials.

Since the topic has been investigated for decades, many researchers have summarized the materials for the removal [5,22] and sensing [23,24] of VOCs. Most references have been reviewed based on a specific category of material, such as TiO₂ [13,25,26], graphene-based materials [27], zinc indium sulphide [28] and silica-nanosphere-based materials [29] etc., or focusing on the catalytic oxidation processes in a specific situation such as low temperature [30], visible light [31,32], or based on a summary from the perspective of various VOCs [5]. However, few have been done from a material perspective together with the consideration of applications on buildings. In this review paper, we do not discuss adsorption-based materials because there are already existing review papers [5,9]. Since the performances of the catalytic oxidations are different for various materials, it is reasonable to categorize by their physiochemical characteristics, which will further affect their applications on buildings. Therefore, this review proposed a novel summary on the materials for catalytic removal of VOCs and their applications on buildings (Figure 2). Morphology, synthesis, performance, and their applications will be explained in detail. This review will further contribute to the applications of photocatalysis materials on buildings.

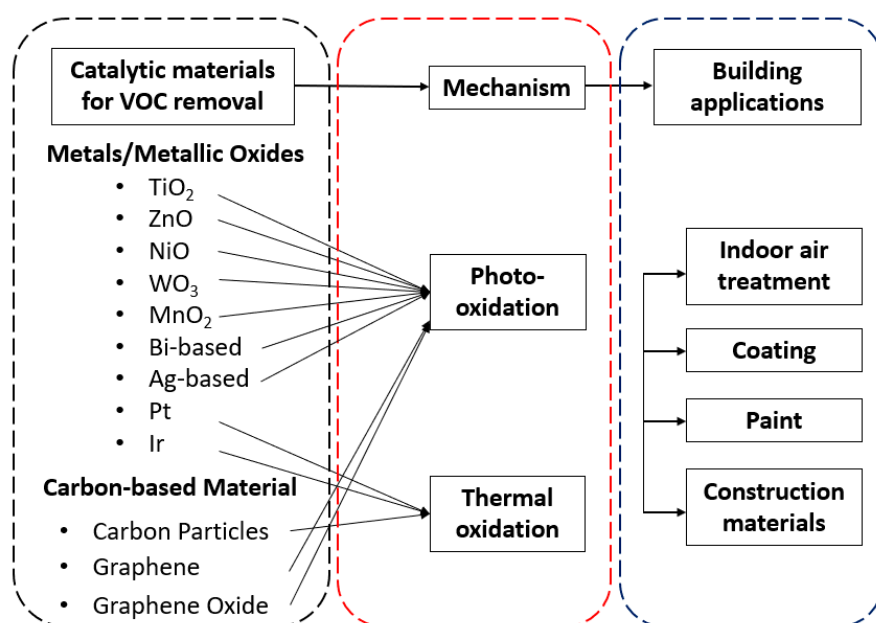


Figure 2. Outline of this review paper.

2. Materials

This review will summarize the materials used for catalytic oxidation of VOCs. The commonly used materials and their characteristics have been listed in Table 1. For this study, catalysts used for the oxidation of VOCs can be classified into two major groups: metallic oxide catalysts and carbon-based materials.

Table 1. Commonly used materials for catalytic removal of VOCs.

No.	Catalytic	Category	VOC	Nanomaterial	Morphology	Medium	Doping Concentration	Synthesis	Ref.
1	Photo-	TiO ₂	Trichloro-ethylene	nanostructured TiO ₂ particles	Primary particle size: 2.3–30 nm, secondary particle size: 100–900 nm	titanium isopropoxide	water concentrations: 2.3, 0.3, 0.27, and 0.18 M	low-temperature synthesis, modified sol-gel method	[33]
2	Photo-	TiO ₂	Toluene	Titanium isopropoxide	Primary particle size: 11 nm	isopropanol–water solution	2.5 mL H ₂ O, 25 mL ethanol, 150-mL (hydrothermal)	sol-gel synthesis, thermal & hydrothermal methods	[34]
3	Photo-	TiO ₂	Toluene	TiO ₂ thin films	particle sizes less than 100 nm, monocrystalline nanodiamond	Titanium (IV) tetraisopropoxide (TTIP) (Ti(OCH(CH ₃) ₂) ₄) and water		detonation method (purchased from microdiamant)	[35]
4	Photo-	TiO ₂	Toluene, acetaldehyde	TiO ₂ nanotubes (TNT) & nanoparticles (TNP) film; commercial TiO ₂ (P25)	average surface area of 50 m ² g ⁻¹ , primary particle size: 20–30 nm, channel pores diameter: 40–60 nm, tube length: 9.5 (±0.9) μm.	[TNP] Ethanol [TNT] ethylene glycol electrolyte	[TNP] 0.15 g/mL [TNT] 1st anodization: 0.5 wt% NH ₄ F and 3 wt% H ₂ O; 2nd: 0.3 wt% NH ₄ F and 1 wt% H ₂ O.	[TNP] doctor-blade method [TNT] two-step electrochemical anodization	[36]
5	Photo-	TiO ₂	Toluene	Ti-foil (99.7%, 0.25 mm, Aldrich, USA)	top and bottom opened structure of which the diameters are 100 nm and 50 nm, respectively NP@DNT films of 15 (±2) μm	ethylene glycol solution containing 0.25 wt% NH ₄ F and 0.3 vol% distilled water		potentiostatic anodization method	[37]
6	Photo-	TiO ₂	Hexane, methanol	anatase and rutile TiO ₂ (0.1 mol)	Surface area between 39 to 84 m ² /g (given in table)	1.5 mol anhydrous Ethanol, water–ethanol solution containing 1 mol ethanol with a ratio of water:butoxide = 50:1.	aqueous HNO ₃ solution of various concentration (0.1–1.0 mol/L) with the ratio of solid (g): liquid (mL) = 1:10	hydrothermal method	[38]
7	Photo-	TiO ₂	Toluene	Anatase/brookite/rutile tricrystalline TiO ₂	amorphous TiO ₂ suspension	HNO ₃ solution (65%)	The molar ratios of HNO ₃ to TBOT (RHNO ₃) were varied from 0.2 to 1.2 at intervals of 0.2 by varying the volume of HNO ₃ solution.	low-temperature hydrothermal method	[39]
8	Photo-	TiO ₂	Toluene	co-alloying TiO ₂	fine bright yellow powder, primary particles diameter: 1–2 μm	TiCl ₄ reacted with NbCl ₅ and urea in an ethanol solution	toluene concentrations: 1–5 ppm; relative humidity: 25–65%; air velocity: 0.78–7.84 cm/s; irradiancy: 42–95 W/m ² .	urea-glass synthesis	[40]
9	Photo-	TiO ₂	Isopropyl alcohol	Hybrid Cu _x O/TiO ₂ Nanocomposites	Commercial TiO ₂ (rutile phase, 15 nm grain size, 90 m ² /g specific surface area)	CuCl ₂ solution, NaOH and glucose solutions (reduce & control the Cu ^I /Cu ^{II} ratio)	10 mL of CuCl ₂ solution. Weight fraction of Cu: TiO ₂ is 1 × 10 ³ : 2 × 10 ² .	simple impregnation method	[41]
10	Photo-	TiO ₂	Toluene	commercial TiO ₂ (P25)	Platinum nanoparticles in the size of 1–3 nm were clearly deposited on the surface of TiO ₂	0.5 wt% Pt and 30 mM fluoride for VOC degradation	sodium fluoride (10, 30, and 50 mM) and Pt (0.1, 0.5, and 1 wt%)	photo deposition method	[42]

Table 1. Cont.

No.	Catalytic	Category	VOC	Nanomaterial	Morphology	Medium	Doping Concentration	Synthesis	Ref.
11	Photo-	TiO ₂	Toluene	hybrid nanomaterial Pt-rGO-TiO ₂	TiO ₂ nanopowder: commercial P25 (Degussa).	ethanol-water	0.1, 0.5, 1 and 2 wt% Pt-rGO-TiO ₂ nanocomposite catalysts	solvothermal method	[43]
12	Photo-	TiO ₂	Toluene	Composites ACFE 0.5 mL tetra-butyl titanate (97 wt%)	Diameter: 12 µm, pore size: 32 µm.	Polytetrafluoroethylene (Teflon)-lined stainless-steel autoclaves	1.0, 2.0, 3.5 and 5.0 l of toluene were injected into the above reactor	Purchased ACFE,	[6]
13	Photo-	TiO ₂	Formaldehyde, trichloro-ethylene	TiO ₂ nanoparticles	BET area: 392 m ² g ⁻¹ , micro mean pore size: 0.6 nm	8 wt% DAPs		incipient wetness impregnation, freeze-drying, or mechanical mixing	[44]
14	Photo-	Zinc oxide	Toluene	ZnAl ₂ O ₄ nanoparticles	commercial P25 powder (reference) TiO ₂ nanoballs in anatase phase	[solvothermal synthetic] Al(NO ₃) ₃ ·9H ₂ O (2 mmol), Zn(NO ₃) ₂ ·6H ₂ O (1 mmol), ethylene glycol (30 mL) [citrate precursors] 0.01 M Zn(NO ₃) ₂ ·6H ₂ O, 0.02 M Al(NO ₃) ₃ ·9H ₂ O, 100 mL DI water [hydrothermal] an equimolar amount of Zn(NO ₃) ₂ ·6H ₂ O (2 mmol), Al(NO ₃) ₃ ·9H ₂ O (4 mmol), urea[CO(NH ₂) ₂] (20 mmol) and deionized water (80 mL)		solvothermal, citrate precursor, hydrothermal methods	[45]
15	Photo-	Ni oxide	Toluene	Nitrogen-doped carbon nanotubes (NCNTs) supported NiO(NiO/NCNTs)	NCNTs: tubular structure, 20 nm-diameter; NiO: crystallite, 3–10 nm	catalyst and pyridine and/or 3-(aminomethyl)pyridine	volume ratio of pyridine to 3-(aminomethyl)pyridine: 5, 3, 1 and 0	Chemical vapor deposition method	[46]
16	Photo-	WO ₃	H ₂ O ₂	Nano-diamonds combined with WO ₃	ND: ca. 4–6 nm diameter	WO ₃ (Aldrich)	0.5–16 wt% ND contents	Simple dehydration condensation	[47]
17	Photo-	Manganese Oxide	Benzene, Toluene, Ethylbenzene, Xylenes	Manganese Oxide and Copper	KMnO ₄ solution (OMS-2); Mn(CH ₃ COO) ₂ ·4H ₂ O (AMO)	Mn(CH ₃ COO) ₂ solution (OMS-2); KMnO ₄ (AMO);		a simple refluxing method	[48]
18	Photo-	Manganese Oxide	Formaldehyde indoors	manganese oxide	Shown in SEM images	ethanol solution of manganese acetate tetrahydrate (Mn(CH ₃ COO) ₂ ·4H ₂ O)	Mn(CH ₃ COO) ₂ ·4H ₂ O: PAN-ACNF 0.5–20 wt.%		[49]
19	Photo-	Bi-based compounds	Acetone, toluene	Bi ₂ WO ₆	CQDs: high dispersion, uniform size of 3–5 nm in diameter	carbon quantum dots (CQDs)	adding 1.0–6.0 g of CQDs	Hydrothermal synthesis	[50]
20	Photo-	AgBr	methyl orange	AgBr	monoclinic WO ₃ substrate, face-centered cubic AgBr nanoparticles: crystalline sizes less than 56.8 nm.	WO ₃	AgBr contents were respectively obtained and defined as TA-0.05, TB-0.10, TC-0.15, TD-0.20, TE-0.25, TF-0.30 and TG-0.40.	deposition-precipitation method	[51]
21	Thermal	Platinum	Toluene	Pt/Al ₂ O ₃ -CeO ₂ nanocatalysts	average size: 5–20 nm.	CeO ₂ (10%)/Al ₂ O ₃ , 2.8 g Ce(NO ₃) ₃ ·6H ₂ O, 100 mL distilled water	ceria loading of 10, 20 and 30%	wet impregnation method	[52]

Table 1. Cont.

No.	Catalytic	Category	VOC	Nanomaterial	Morphology	Medium	Doping Concentration	Synthesis	Ref.
22	Thermal	Platinum	benzene	Pt/Al ₂ O ₃	Pt particle sizes between 1.2–2.2 nm	H ₂ PtCl ₆ ·6H ₂ O	Pt/A I ₂ O _{3-x} ; x: pH value of 7.0, 9.0 and 11.0	modified ethylene glycol (EG) reduction approach	[53]
23	Thermal	Platinum	Formaldehyde (HCHO)	Pt/TiO ₂ /Al ₂ O ₃	BET area from 16.5 to 182.5 m ² /g	(NH ₄)[TiO(C ₂ O ₄) ₂]	The platinum loading: 0.62, 1.26, 1.19 and 1.25 gm ⁻²	Electro-deposition technology	[54]
24	Thermal	Silica-iridium	Toluene	chloride-ion free iridium acetylacetonate, Ir(AcAc) ₃	~5 to 27 nm	SiO ₂ Degussa Aerosil 200	Size of iridium particles: ~5 to 27 nm (calcination temperature 350–750 °C)	incipient wetness impregnation	[55]
25	Thermal	Carbon	benzene, toluene, ethylbenzene, and oxylene	Pt/carbon nanotube (CNT) Multiwalled carbon nanotubes (MWCNT)	CNTs: 20–50 nm column diameters MWCNTs: 20–50 nm diameters	acid treatment using HF, H ₂ SO ₄ , and HNO ₃	Pt content in the catalysts ranging from 10 to 30 wt%.	a molecular-level mixing method	[56]
26	Photo-	Carbon based	Volatile Aromatic Pollutant	TiO ₂ -graphene	Shown in SEM image	An ethanol-water solvent	P25_GR with weight addition ratios of 0.2, 0.5, 1, 2, 5, 10, and 30% GR.	facile hydrothermal reaction	[57]
27	Photo-	Carbon-based	methanol	graphene oxide, reduced graphene oxide, and few-layer graphene	BET area (m ² /g): rGO+TiO ₂ : 49.34, GO+TiO ₂ : 43.79, G+TiO ₂ : 41.54	Polyacrylonitrile	a polymer concentration of 5% (w/w) in N,N-dimethylformamide.	hydrothermal method (reduced graphene oxide); others purchased	[58]

2.1. Metallic Oxides

2.1.1. Titanium Dioxide (TiO₂)

With a wide band-gap energy, durability against photo-corrosion, low toxicity, and low cost, TiO₂ is regarded as the most efficient and applicable material [59]. In 1972, the photoelectrochemical decomposition of water under irradiation with light on TiO₂ was found for the first time [60]. Photocatalysis performances of TiO₂ and its derivatives were studied over decades.

The photocatalyst performance can be affected by the structure and morphology [33] and treatments [34] of the TiO₂ particles. Maira et al. [33] investigated the effects of different synthesis parameters on the size and morphology of the TiO₂ particles, and the trichloroethylene degradation over TiO₂ catalyst exhibits a maximum at a primary particle size of 7 nm. They [34] further compared the treatments applied to an amorphous TiO₂ precursor for obtaining nanosized TiO₂ particles. Compared to the anatase TiO₂ treated with the thermal method, the one with the hydrothermal method can improve the photo activity and showed a higher number of hydrogen-bonded hydroxyl groups that are more stable under RT outgassing and a stronger adsorption ability on Benzaldehyde.

TiO₂ with different morphologies showed different photocatalytic performances. Lee et al. [35] developed novel nanostructured gas filtering systems with TiO₂ thin films using atomic layer deposition (ALD) for VOCs, which showed a superior efficiency for the toluene adsorption. Weon and Choi [36] compared the photocatalytic activities of TiO₂ nanotubes (TNT) and TiO₂ nanoparticles (TNP) film during the repeated cycles of photocatalytic degradation of gaseous toluene and acetaldehyde. Figure 3a,b shows the TEM images of fresh TNP and TNT, respectively. The photocatalytic activity of TNT showed only moderate reduction after the five cycles of toluene degradation, whereas TNP underwent rapid deactivation as the photocatalysis cycles were repeated, even in a more oxidizing atmosphere (Figure 3c,d). With a highly-ordered open channel structure, TNT can easily supply O₂ molecules to the active sites with less mass transfer limitation, which prevents the TNT surface from carbonaceous residues accumulation. It indicated that the structural characteristics of TNT are highly advantageous in preventing the catalyst deactivation during the photocatalytic degradation of aromatic compounds. Weon et al. [37] later synthesized freestanding doubly open-ended TiO₂ nanotubes (DNT) film, which exhibited higher activity and durability for the photocatalytic degradation of gaseous acetaldehyde and toluene than TiO₂ nanotubes. If the freestanding DNT film was additionally loaded with TiO₂ nanoparticles (NP@DNT) in the inner wall, the activity for VOC degradation will be increased by 1.3 and 1.8 times of those for bare DNT and bare TNT, respectively. However, the loading of TiO₂ nanoparticles on TiO₂ nanotubes showed a lower activity than bare TNT.

TiO₂ primarily exists in three crystal phases: anatase, brookite and rutile. Among them, the anatase form appears to be the most photoactive and the most practical for widespread environmental applications [25]; the brookite was once regarded to not be suitable as a photocatalyst [25,61], and later the successful synthesis of nanostructured brookite was showed to greatly enhance the photocatalytic performance [62]. Wu et al. [38] investigated the synergetic effect between anatase and rutile nanoparticles in gas-phase photocatalytic oxidations of hexane and methanol. The synergetic effect could be more significant if anatase and rutile particles are closely contacted. The long-term experiment proves the stability of the photocatalyst activity, and it cannot be improved by sulfation, which works well for the single-phase anatase TiO₂.

The tricrystalline TiO₂ shows higher photocatalytic activity and durability toward gaseous toluene than bicrystalline TiO₂ [39]. To remove toluene from the indoor air efficiently and economically, Chen et al. [39] synthesized anatase/brookite/rutile tricrystalline TiO₂ by a low-temperature hydrothermal route with HNO₃. As shown in Figure 4a, the one with RHNO₃ = 0.8 (80.7% anatase, 15.6% brookite and 3.7% rutile) had the highest photocatalytic activity about 3.85-fold higher than that of P25 TiO₂, which is a widely-used benchmark model photocatalyst coexisting anatase and rutile phases. Moreover, the high activity did not significantly degrade even after five reuse cycles (Figure 4b).

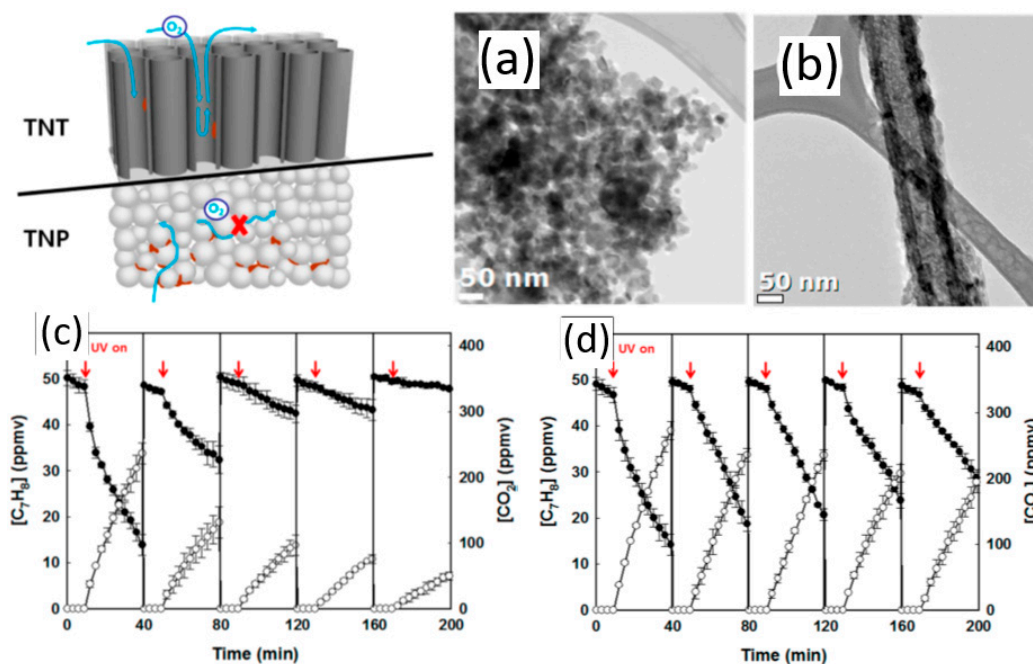


Figure 3. TEM images of fresh (a) TNP and (b) TNT; repeated photocatalytic degradation cycles of gaseous toluene on (c) TNP and (d) TNT in the air (●: [Toluene], ○: [CO₂]) [36]. (adapted from [36], with permission from American Chemical Society, 2019).

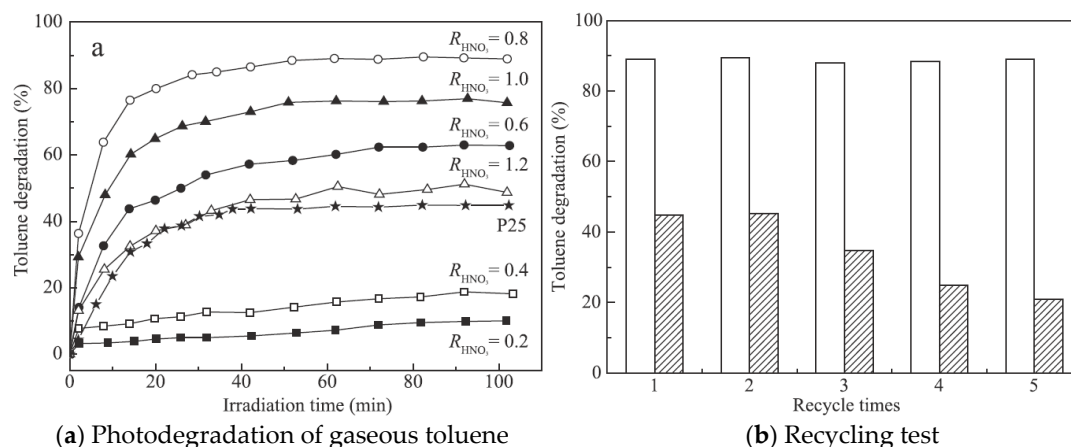


Figure 4. Comparison results between TiO₂ and P25 for (a) photodegradation rate of gaseous toluene and (b) recycling test over tricrystalline TiO₂-0.8 (blank) and P25 (filled) for five repeat uses [39]. (adapted from [39], with permission from Elsevier, 2019).

However, the leading semiconductor photocatalyst, TiO₂, also suffers from low photocatalytic activity under visible light activation because of its intrinsic wide band gap. Therefore, to increase the efficiency of TiO₂ in the visible light region, TiO₂ is modified with various nanomaterials including other metal oxides [40–42], carbonaceous nanomaterials [43] etc. Zhong et al. [40] developed a TiNbON compound (band energy of 2.3 eV) using urea-glass synthesis as a visible light responsive photocatalytic oxidation material for toluene degradation. Experimental results showed that the visible light-driven catalyst was able to remove up to 58% of the toluene and generated less formaldehyde than the commercial TiO₂ with reasonable durability and stability. Qiu et al. [41] grafted nano-Cu_xO clusters onto TiO₂ to generate an excellent risk-reduction material in indoor environments (Figure 5a). The Cu^{II} in the Cu_xO clusters enables TiO₂ to protoxidize VOCs under visible light efficiently, and it has the antimicrobial properties under dark conditions due to Cu^I species. Therefore, the efficient reduction of VOCs and antipathogenic activity could be achieved in hybrid Cu_xO/TiO₂ nanocomposites with a

proper proportion of Cu^{I} and Cu^{II} in Cu_xO . As shown in Figure 5b, the $\text{Cu}_x\text{O}/\text{TiO}_2$ sample shows a superior photocatalytic activity over the $\text{TiO}_{2-x}\text{N}_x$ sample with high quantum efficiencies and stability under long-term light irradiation.

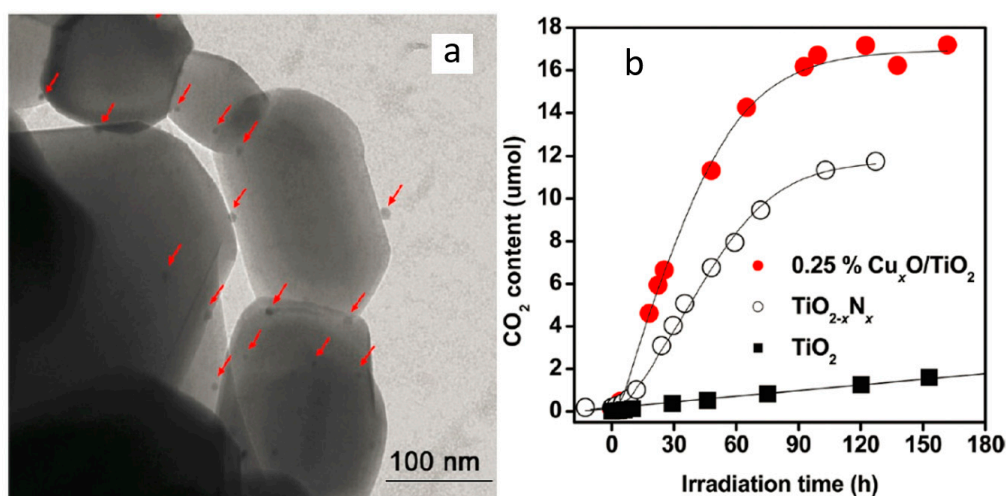


Figure 5. (a) TEM images of the 0.25% $\text{Cu}_x\text{O}/\text{TiO}_2$ sample. Cu_xO clusters (marked by red arrows) were highly dispersed on the TiO_2 surfaces; (b) comparative studies of CO_2 generation over bare TiO_2 , $\text{TiO}_{2-x}\text{N}_x$, and 0.25% $\text{Cu}_x\text{O}/\text{TiO}_2$ samples under the same conditions [41]. (adapted from [41], with permission from American Chemical Society, 2019).

Jo et al. [63] applied an annular reactor coated with unmodified or nitrogen (N)-doped TiO_2 for VOCs removal in the indoor environment. The photocatalytic technique using N-doped TiO_2 was much superior to that for unmodified TiO_2 , and it can remove above 90% for four target compounds (ethyl benzene, o,m,p-xylenes) under conditions of less humidified environments, including a typical indoor comfort range (50–60%). Weon et al. [42] modified TiO_2 nanoparticles with Pt and fluoride and tested their durability for toluene removal. Figure 6a shows the HR-TEM of the composite. Although Pt/ TiO_2 had a higher photocatalytic degradation activity than bare TiO_2 , it could be deactivated rapidly during repeated cycles. Among them, F- TiO_2/Pt showed the highest photocatalytic activity and durability for toluene degradation (Figure 6b).

Li et al. [43] introduced a hybrid nanomaterial Pt-rGO- TiO_2 (Figure 7a). With a broad light wavelength absorption (800–2500 nm), the highly-active photo-thermal responsive catalyst can decompose VOCs efficiently under IR irradiation. As shown in Figure 7b, the light intensity can affect the efficiency of Pt-rGO- TiO_2 composites on the conversion of toluene and the yield of CO_2 . If the infrared irradiation intensity is $116 \text{ mW}/\text{cm}^2$, a maximum photo-thermal conversion efficiency of 14.1% would be achieved with a significant toluene conversion of 95% and a CO_2 yield of 72%, and a nearly 50 h stability duration.

Metal oxides also synthesized with adsorption materials to enhance their photocatalysis performances. Li et al. [6] firstly fabricated nanostructured $\text{TiO}_2/\text{activated carbon fiber-felt}$ (TiO_2/ACFF) porous composites by the in-situ deposition of TiO_2 microspheres on the carbon fibers in ACFF. Figure 8a shows hierarchical nanostructures constructed by nanocrystals of TiO_2 microspheres. Due to the synergetic effects of nanostructured TiO_2 and ACFF, the TiO_2/ACFF porous composites possess excellent adsorption and photodegradation properties for toluene. The ACFF in the TiO_2/ACFF porous composites significantly enhances photocatalytic property for toluene by hindering the recombination of electron-hole pairs, reducing the TiO_2 band gap energy to 2.95 eV and accelerating toluene adsorption.

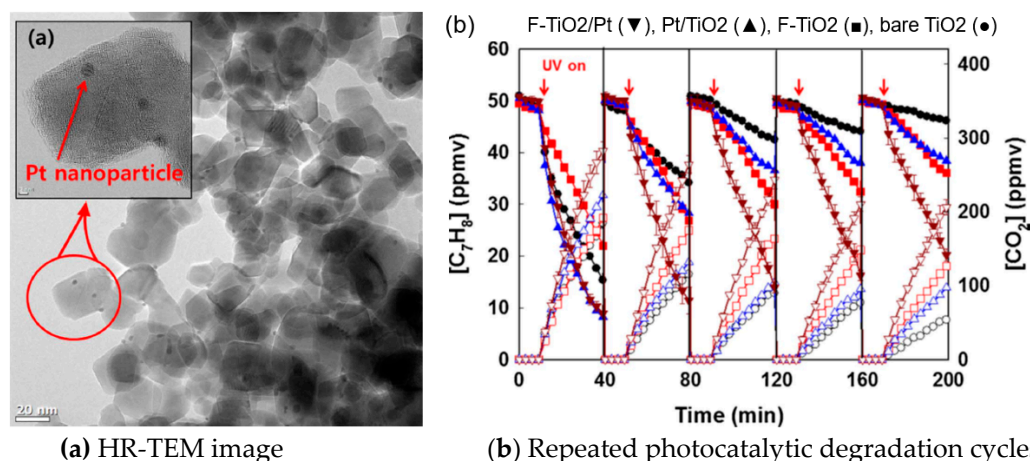


Figure 6. (a) HR-TEM image and (b) repeated photocatalytic degradation cycles of gaseous toluene on F-TiO₂/Pt [42]. (adapted from [42], with permission from Elsevier, 2019).

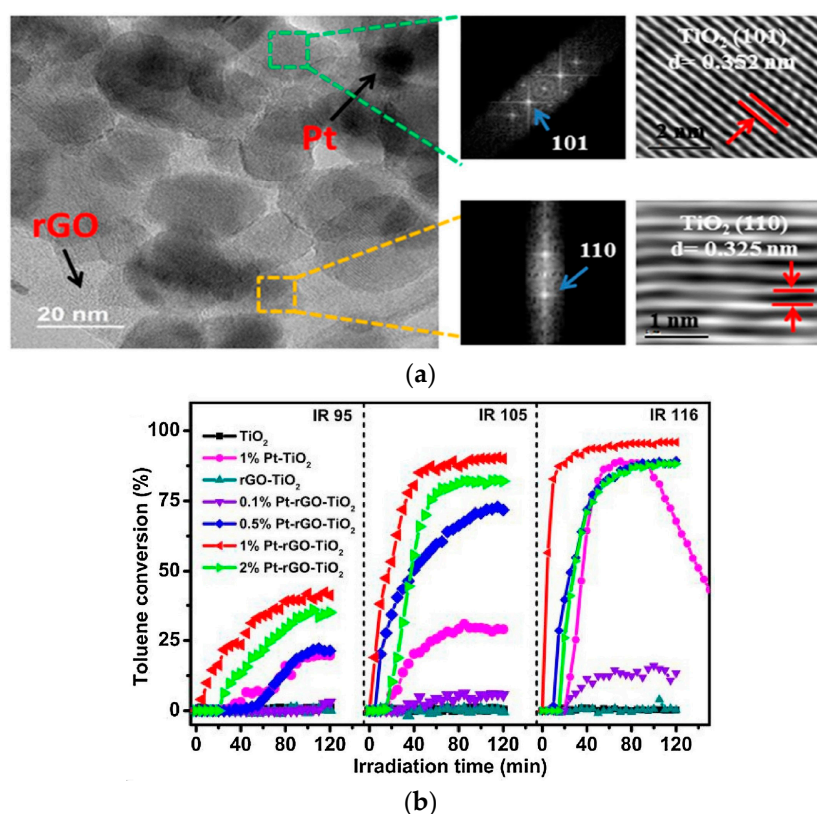


Figure 7. (a) High-angle annular dark-field scanning transmission electron microscopy images and HRTEM of 1% Pt-rGO-TiO₂; (b) time course of toluene conversion over TiO₂, 1% Pt-TiO₂ and x% Pt-rGO-TiO₂ (x = 0, 0.1, 0.5, 1 and 2) under IR irradiation with various light intensities (95, 106 and 116 mW/cm²) [43]. (adapted from [43], with permission from Elsevier, 2019).

Similar combination can be found in Ref. [44], where the TiO₂ nanoparticles (Ti-NP) were synthesized with decahedral anatase particles (DAPs), and their photocatalytic activity of TiO₂/zeolite hybrids for VOCs oxidation was analyzed. TiO₂ nanoparticles of 5 nm, DAPs of ca. 100 nm, and 1.0 μm clusters of TiO₂ made of 15 nm mean particle size characterized the three types of TiO₂. The incorporation of TiO₂-NP into the zeolitic material led to composites with around 10 times more photoactivity than the single titania particles. Elfalleh et al. [64] used TiO₂-impregnated polyester and glass fiber to address the photocatalytic degradation of aldehydes (air-solid interface). Also, the TiO₂ nanoparticles were

fixed by the glass fiber tissue coated with colloidal silica in reactors to photo-catalytically remove isovaleraldehyde [65] and isovaleric acid [66].

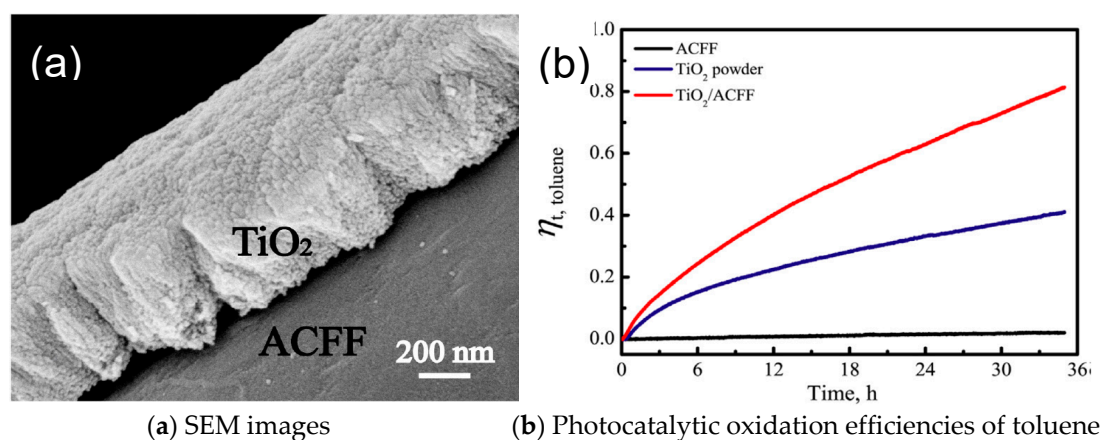


Figure 8. (a) SEM images and (b) Photocatalytic oxidation efficiencies of toluene as function of photocatalytic time under UV irradiation with TiO_2/ACFF porous composites [6]. (adapted from [6], with permission from Elsevier, 2019).

2.1.2. Zinc Oxide

As an alternative to TiO_2 , zinc oxide is considered to be a fast and efficient chemical decontamination of VOCs [67]. Li et al. [45] compared three synthetic methods to prepare ZnAl_2O_4 for the photocatalytic degradation of gaseous toluene: solvothermal, citrate precursor and hydrothermal methods, whose SEM figures can be found in Figure 9a–d. The photocatalytic performances of the ZnAl_2O_4 samples synthesized by facile solvothermal method exhibited about 90% photocatalytic efficiency of toluene (Figure 9e). The photocatalytic oxidation of gaseous pollutant over UV-illuminated ZnAl_2O_4 is a promising technique for air purification.

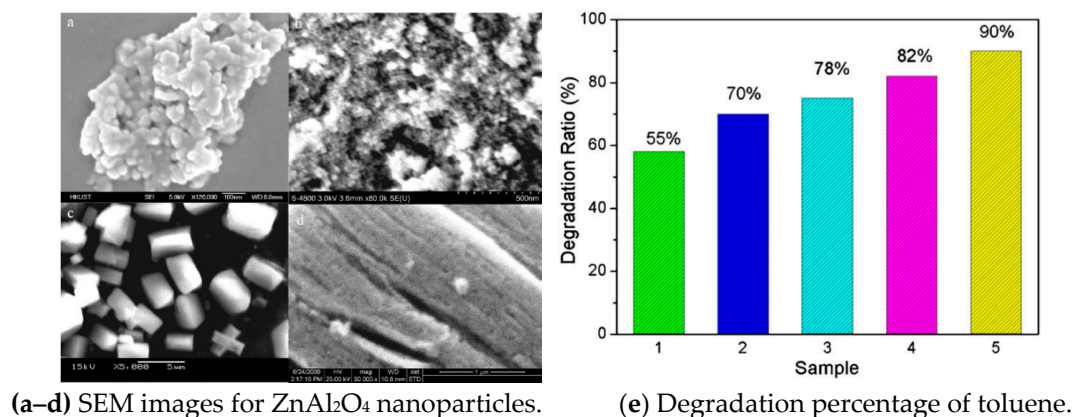


Figure 9. SEM images for ZnAl_2O_4 nanoparticles synthesized with (a) hydrothermal, (b) citrate precursors, (c,d) solvothermal synthetic methods. (e) The degradation percentage of toluene among 1 (ZnAl_2O_4 nanoparticles + citrate precursors), 2 ($\text{P}25 \text{ TiO}_2$), 3 (ZnAl_2O_4 nanoparticles + hydrothermal), 4 (TiO_2 nanoballs), and 5 (ZnAl_2O_4 nanoparticles + solvothermal synthetic) samples under UV illumination [45]. (adapted from [45], with permission from Elsevier, 2019).

2.1.3. Nickel Oxide

Jiang et al. [46] compared the catalysis performance of nitrogen-doped carbon nanotubes (NCNTs) supported by NiO (NiO/NCNTs) with different pyridine volume ratios (Figure 10a–d). The oxygen adspecies concentration and low-temperature reducibility of NiO/NCNTs increased with increasing

the doped graphitic-like N(NG) content of NCNTs (Figure 10e). The optimized NiO/NCNTs-d catalyst with NG content of 6.22 at.% can achieve a completed conversion of toluene at 248 °C, and has a TOF value of nearly 10 times NiO/CNTs at 160 °C.

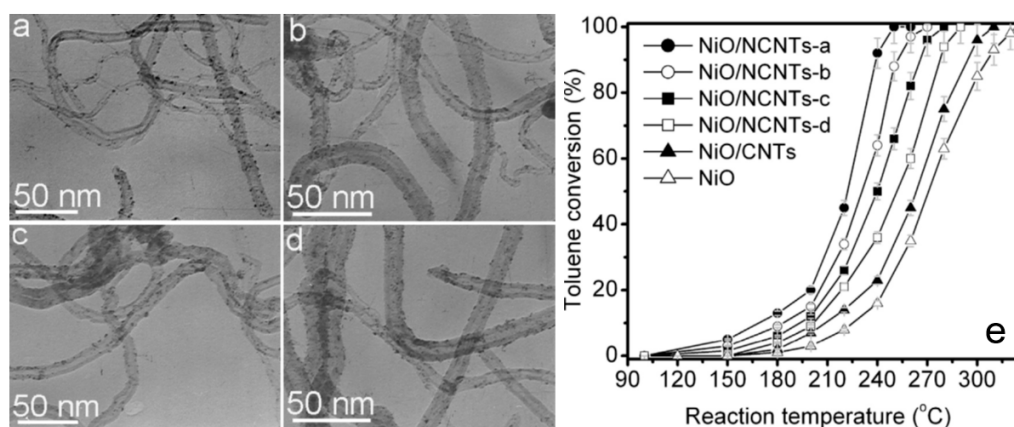


Figure 10. TEM images of NiO/NCNT catalysts with the pyridine to 3-(aminomethyl) pyridine volume ratios of (a) 5, (b) 3, (c) 1 and (d) 0; and (e) their toluene conversion vs. reaction temperatures against those of NiO/CNTs [46]. (adapted from [46], with permission from Elsevier, 2019).

2.1.4. Tungsten Trioxide

Kim et al. [47] combined nanodiamond (ND) with WO_3 (as an alternative co-catalyst for Pt) to degrade VOCs under visible light. NDs-loaded WO_3 showed a highly enhanced photocatalytic activity for the degradation of acetaldehyde (~17 times higher than bare WO_3), which is more efficient than other well-known co-catalysts (Ag, Pd, Au, and CuO) loaded onto WO_3 and comparable to Pt-loaded WO_3 . The surface conductivity of ND loaded on WO_3 plays a critical role in the overall photocatalysis. The photocatalytic activity of NDs/ WO_3 was higher than that of WO_3 loaded with other carbon-based co-catalysts (graphene oxide or reduced graphene oxide).

2.1.5. Manganese Oxide

Genuino et al. [48] synthesized cryptomelane-type octahedral molecular sieve (OMS-2) manganese oxide, amorphous manganese oxide (AMO), and mixed copper manganese oxide ($\text{CuO}/\text{Mn}_2\text{O}_3$) nanomaterials, together with commercial MnO_2 . Due to complex reasons including structure, morphology, hydrophobicity, and redox properties, OMS-2, AMO, and $\text{CuO}/\text{Mn}_2\text{O}_3$ showed higher oxidative activities than the commercial MnO_2 . Miyawaki et al. [49] developed a novel hybrid catalyst for long-lifetime formaldehyde removal, which deposits manganese oxide (MnO_x) catalysts on a polyacrylonitril-based activated carbon nanofiber (PAN-ACNF) support. The combination of MnO_x with PAN-ACNF induced synergic effects on the formaldehyde removal performance, which doubly improved the performance of PAN-ACNF in either dry or humid conditions without UV light. The manganese oxides were also interacted with cerium oxide [68] and CoAl mixed oxides [69] for a better catalytic removal of gaseous VOCs.

2.1.6. Bi-Based Compounds

Qian et al. [50] incorporated highly stable carbon quantum dots (CQDs) with Bi_2WO_6 to sufficiently photocatalytic removal of VOCs. The CQDs/ Bi_2WO_6 photocatalyst can extend the absorption into visible light region and improve the photoexcited charge separation in comparison with pristine Bi_2WO_6 . This photocatalyst showed higher photocatalytic oxidation activities towards acetone and toluene under both UV-vis and visible light irradiation.

2.1.7. Ag-Based Compounds

Kobayashi et al. [70] investigated the photocatalytic activity of AgBr. AgBr(N₂) prepared at 250 °C showed the highest H₂ generation activity, although larger crystallites of Ag were observed. Cao et al. [51] synthesized a novel AgBr/WO₃ composite photocatalyst by loading AgBr on WO₃ substrate via the deposition–precipitation method. AgBr/WO₃ displays good photocatalytic activity under visible light ($\lambda > 420$ nm).

2.1.8. Platinum Supported Material

Abbasi et al. [52] prepared Pt/Al₂O₃–CeO₂ nanocatalysts with Pt loading of 1% and ceria loading of 10, 20 and 30% to be utilized in catalytic oxidation of BTX (Figure 11a). The results of toluene oxidation indicated that the synthesized nanocatalysts were highly active and able to remove nearly 100% of toluene and xylene and about 85% of benzene as representative VOCs (Figure 11b).

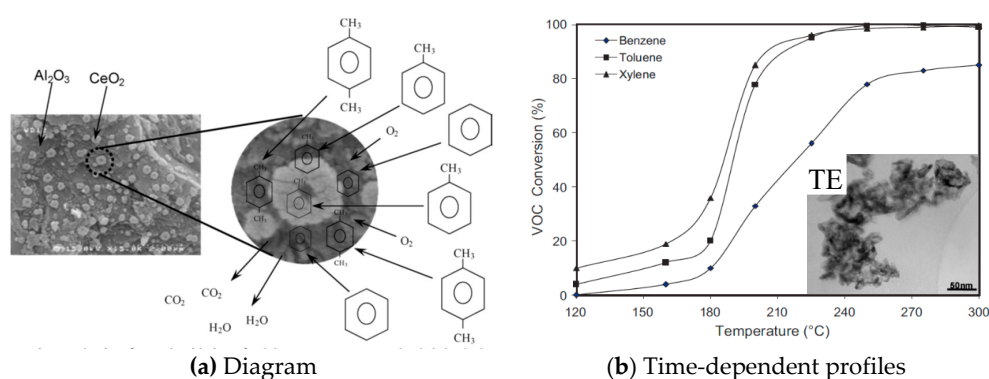


Figure 11. (a) Reaction mechanism for total oxidation of VOCs over nanostructured Pt/Al₂O₃–CeO₂ catalysts. (b) Comparison of catalytic performance of synthesized Pt (1 wt%)/Al₂O₃–CeO₂ (30 wt%) nanocatalyst for total oxidation of benzene, toluene and xylene [52]. (adapted from [52], with permission from Elsevier, 2019).

Chen et al. [53] prepared a series of Pt/Al₂O₃ catalysts by modified ethylene glycol (EG) reduction approach with Pt particle sizes between 1.2–2.2 nm. Pt/Al₂O₃ catalyst with 1.2 nm Pt size exhibited optimum catalytic oxidation activity of benzene at 145 °C. The catalysts showed excellent adaptability for different VOCs and durability for benzene oxidation during the long-term continuous test, whether in dry air or in the coexistence of CO₂, cyclohexane or H₂O. Wang et al. [54] prepared a Pt/TiO₂/Al₂O₃ catalyst on an anodic alumite plate for the catalytic decomposition of formaldehyde at ambient temperature. The developed catalyst has good activity on decomposing HCHO at ambient temperature. With quick activation of absorbing oxygen, the Pt/TiO₂/Al₂O₃ catalyst showed a high activity towards the catalytic decomposition of formaldehyde at ambient temperature.

2.1.9. Iridium Particles

Other oxides were also investigated, for example, Schick et al. [55] synthesized iridium particles supported on silica for the total oxidation of VOCs, and the catalytic activity increases when the iridium oxide particle size decreases.

2.2. Carbon-Based Materials

2.2.1. Carbon-Based

Joung et al. [56] fabricated a novel Pt/carbon nanotube (CNT) catalyst using a molecular-level mixing method (Figure 12a), and its performance on oxidation of benzene, toluene, ethylbenzene, and o-xylene (BTEX) was investigated at temperatures ranging from 40 to 150 °C (Figure 12b). The oxidation activity was presumably promoted because of the higher surface BTEX concentration afforded by the

adsorption capability of multiwalled carbon nanotubes. The catalyst was characterized by its unique hydrophobic property, which facilitates the conversion of BTEX with high activity at relatively low temperatures and was unaffected by moisture in the system.

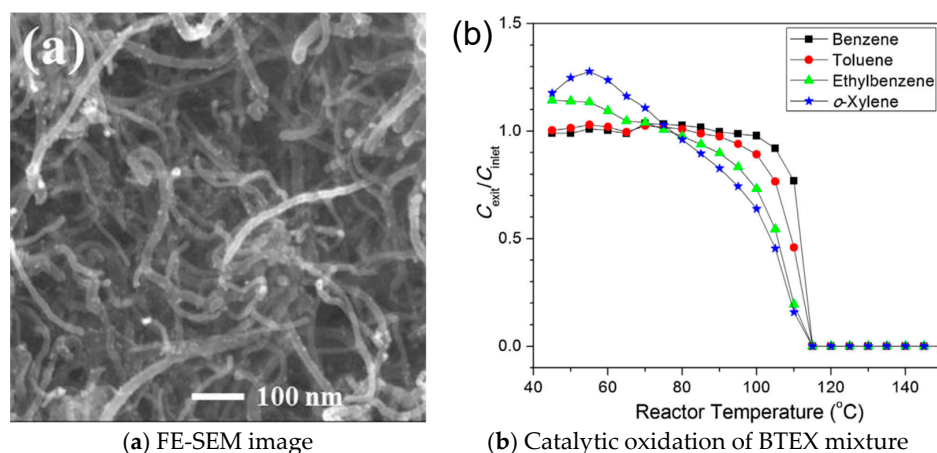


Figure 12. (a) Field emission scanning electron microscopy image and (b) catalytic oxidation of BTEX mixture as a function of reactor temperature over 30 wt% Pt/CNT catalyst [56]. (adapted from [56], with permission from Elsevier, 2019).

2.2.2. Graphene and Graphene Oxide (GO)

Graphene and graphene oxide (GO) have been considered as a proficient matrix for sorption gaseous pollutants due to their advanced properties including facile synthesis method, high surface area, robust pore structure, lightweight, high chemical stability, and high thermal stability [71]. In recent years, great effort has been put into combining graphene/GO with various metal oxides (including TiO₂, WO₃, SnO₂ and CO₃O₄ etc.) to improve the efficiency of VOCs' removal. Even with unique structural and electronic properties, the metal oxide (e.g., TiO₂/graphene) was found to be the same in essence as other TiO₂/carbon (carbon nanotubes, fullerenes, and activated carbon) composite materials with regards to the enhancement of photocatalytic activity of TiO₂ [57]. Since GO can be readily prepared from low-priced graphite materials on a huge scale, the usage of GO-based hybrid multifunctional materials should be much more profitable than that of other expensive nanomaterials such as functionalized carbon nanotubes [71].

Zhang et al. [57] prepared the nanocomposites of TiO₂/graphene via a facile hydrothermal reaction of graphene oxide and TiO₂ in an ethanol water solvent. This nanocomposite showed much higher photocatalytic activity and stability than bare TiO₂ toward the gas-phase degradation of benzene, and the higher weight ratio in TiO₂/graphene will decrease the photocatalytic activity. The photocatalytic efficiency can be strongly affected by the structure of graphene-based composites. Roso et al. [58] compared the performances of three graphene-based co-catalysts (graphene oxide, reduced graphene oxide, and few-layer graphene) on methanol gas-phase photooxidation. Among them, the reduced graphene oxide gave the best performance on degrading methanol with a higher rate.

3. Applications on Buildings

Photocatalysts can be applied on construction materials; their superior photoactivated properties can efficiently reduce or abate the harmful VOCs under UV light irradiation. These materials allowed both to degrade polluting compounds at the materials surface and to decrease maintenance costs thanks to their self-cleaning properties. As a main function for the self-cleaning applications, these materials such as TiO₂ were coated on the surface or mixed with the building materials including glass, mortars, stone [72], asphalt and concrete [73,74], etc. Table 2 summarized the common applications of photocatalytic materials for VOC removal on buildings.

Table 2. Applications of photocatalytic materials for VOC removal on buildings.

No.	Catalytic	Applications	Materials	Comparison & Experiments	Pollutants	Performance	Ref.
1	Thermal	Indoor air purification	Pt/ZnO/SiC	Toluene concentration: 100~500 ppm Loading of Pt nanoparticles: 0.030 wt% (Pt/ZnO/SiC) ~0.017 wt% (Pt/SiC).	Toluene	Toluene was used as a model volatile organic compound and reached complete conversion of up to 100% over the porous tubular Pt/ZnO/SiC material at a filtration velocity of 0.72 m/min within 240 h at 210 °C maintained within 24 h	[75]
2	Photo-	Indoor air purification	Glass fiber tissue supported TiO ₂	Inlet pollutant concentrations (25–300 mg m ⁻³), flow rates (2–8 m ³ h ⁻¹), relative humidity of effluent (5, 30, 50 and 90%), input of the plasma discharge (9–21 kV)	Trichloromethane (CHCl ₃)	Combination of plasma DBD and photocatalysis enhances the removal efficiency	[76]
3	Photo-	Indoor air purification	Ln ³⁺ -TiO ₂	La ³⁺ -TiO ₂ and Nd ³⁺ -TiO ₂ Lanthanide ion dosage of 0.7%, 1.2%, 1.6% and 2.0%	benzene, toluene, ethylbenzene and o-xylene (BTEX)	Highest adsorption ability: 0.7% Ln ³⁺ -TiO ₂ catalysts. TiO ₂ photocatalytic efficiency with the lanthanide ion doping was remarkably enhanced by BTEX removal. The 1.2% Ln ³⁺ -TiO ₂ catalysts achieved the highest photocatalytic activity. Residence time: 72 s using 1.2% La ³⁺ -TiO ₂ catalyst	[77]
4	Photo-	Coating	TiO ₂ thin films	Commercial glasses: Pilkington Activ™ Blue PAB) and Pilkington Activ™ Clear (PAC).	2-propanol	For the 2-propanol oxidation, PAC was found to be more active under UV light due to the larger surface area and higher TiO ₂ particle concentration.	[67]
5	Photo-	Coating	TiO ₂ coated on fiberglass fibers	TiO ₂ coated on carbon cloth fibres, a pilot duct system for experiment	polytetrafluoroethylene	The single-pass removal efficiency ranks: alcohols > ketones > aromatics > alkanes.	[69]
6	Photo-	Coating	TiO ₂	single-layer coating & multilayer TiO ₂ coating	rhodamine B	Degrading self-cleaning ability of analysed coatings caused by ageing processes, and no significant difference between single-layer and multilayer coatings in the long-term	[63]
7	Photo-	Paint	Three self-cleaning photocatalytic paints	Three white commercial photocatalytic paints; expose to UVC lamp, Xenon lamp, LED and fluorescent lamps for 10 h	methyl red, methylene blue	Limited photocatalytic action under visible light	[74]
8	Photo-	Paint	commercial AEROXIDE_TiO ₂ P25 powder	Matrix with nitric acid and H ₂ SO ₄	rhodamine b	Nitric acid causes a decrease in crystallinity and photocatalytic activity, which drops by almost 20%; H ₂ SO ₄ the best candidate for TiO ₂ nanoparticles acid treatment	[75]
9	Photo-	Paint	TiO ₂ microspheres	commercial TiO ₂ particles P25	methylene blue solution	MTiO ₂ : more stable and better photoactivity	[73]

Table 2. Cont.

No.	Catalytic	Applications	Materials	Comparison & Experiments	Pollutants	Performance	Ref.
10	Photo-	Paint	TiO ₂	5% P25-TiO ₂ -intermixed and dip-coated SCAM samples	rhodamine b	TiO ₂ /SCAM: high self-cleaning ability and a robust weathering resistance under UV-A and visible light irradiations.	[71]
11	Photo-	Paint	TiO ₂ coating (PC-S7, Cristal Active)	TiO ₂ (P25) intermixed nanopowder. Experiments: air purifying (indicated by NO _x removal) and self-cleaning (indicated by Rhodamine b removal).	Rhodamine b NO _x	TiO ₂ coating on mortar shows better photocatalytic performances than TiO ₂ intermixed samples on air purifying and self-cleaning properties under both UV-A and visible light (VL) irradiation conditions.	[70]
12	Photo-	Paint	TiO ₂ P25	ZnO Experiments: Paints were exposed to simulated weathering tests in a QUV panel	dye Acid Orange 7	Photocatalytic activity of TiO ₂ increases with weathering time. ZnO: significantly higher photocatalytic activity for initial photoactivity of the unweathered paints but decreased after weathering.	[72]
13	Photo-	Mortar	Mortars containing TiO ₂ and iron oxide pigments	Atmospheric exposure tests and photocatalytic degradation tests were performed.	2-propanol	Iron oxide pigments caused lower photocatalytic activity compared to white mortars. TiO ₂ + mortars has lower soiling in atmospheric exposure	[76]

3.1. Indoor Air Treatment

Indoor air treatment can be used to filter the VOCs from the air to maintain a good quality of air. The filter can be coated with nanomaterials to achieve a better performance for VOCs oxidation. Li et al. [75] prepared a novel Pt/ZnO/SiC filter for the oxidation of toluene; the ZnO coating can disperse Pt nanoparticles and significantly enhance the photocatalytic performance. This filter can achieve complete conversion of toluene at a filtration velocity of 0.72 m/min within 240 h at 210 °C. TiO₂ is more commonly used for application. Zadi et al. [76] evaluated the efficiency of non-thermal plasma and heterogeneous photocatalysis processes for indoor air treatment with glass fiber tissue-supported TiO₂. Various impact factors were analyzed and the combination of plasma DBD and photocatalysis is proved to enhance the removal efficiency. Li et al. [77] found that the photocatalytic efficiency of the TiO₂ catalysts with the lanthanide ion doping was remarkably enhanced by BTEX removal. By comparing different types of Ln³⁺-TiO₂ (La³⁺/Nd³⁺-TiO₂) with various lanthanide ion dosage, the 0.7% Ln³⁺-TiO₂ catalysts showed the highest adsorption ability, and 1.2% Ln³⁺-TiO₂ catalysts achieved the highest photocatalytic activity. Boyjoo et al. [78] also reviewed the catalyst used for air purification in 2017 and concluded that the most commonly used materials were TiO₂ and ZnO, and only very few studies were using other photocatalysts.

3.2. Coating

Photocatalysts have multi-function when coated on the construction materials. For example, the TiO₂ coatings on the glass surface can not only degrade organic dirt and VOCs under light, but also improve the surface hydrophilicity, which can efficiently remove the dust and degraded organic dirt by rainfall [79]. Oladipo et al. [80] reported the photocatalytic activity and energy efficiency of two self-cleaning glasses, Pilkington Activ™ Blue and Pilkington Activ™ Clear. The Clear one was more active than the Blue one towards 2-propanol oxidation under ultraviolet irradiation and showed the best reactivity in the degradation of pre-adsorbed stain under simulated solar irradiation. TiO₂-coated exterior paints can contribute to a 90~98% decane degradation [81].

TiO₂ can be coated to materials in air filters to enhance the photocatalytic oxidation [82]. Zhong et al. [83] compared the performances of two commercially available photocatalytic oxidation air filters, titanium dioxide (TiO₂) coated on fiberglass fibers (TiO₂/FGFs) and TiO₂ coated on carbon cloth fibers (TiO₂/CCFs) in a pilot duct system. The single-pass removal efficiency of these air filters ranks alcohols > ketones > aromatics > alkanes, and various influential factors were analyzed. Jiang et al. [84] coated the ceramic tiles with N, F and Fe ions-doped TiO₂ to photo-catalytically remove NO under visible light. Both air pollutions of inorganic NO and organic compounds can be purified by the ceramic tiles. The coating enables ceramic tiles to have enhanced photocatalytic efficiency, low water adsorption performance, good fastness, and antibacterial capability to reduce the risk of bacterial infection.

To reserve the original aesthetic features of historical and monumental architectures, Munafo et al. [72] applied anatase TiO₂ colloidal suspensions via spray-coating to deposit transparent self-cleaning coatings on stones. Photocatalytic performances of TiO₂-based coatings with one and three spray cycles were compared against that of the untreated travertine. The self-cleaning ability of analyzed coatings was degraded by the ageing processes till reaching low efficiency, and it shows no significant difference between single-layer and multilayer coatings in long-term use. Results seem to encourage the use of nano-structured TiO₂ for preserving stone during time, while the undercoat and new and more stable colloidal TiO₂ is needed.

To achieve a high photocatalytic efficiency and a robust weathering resistant ability, Guo et al. [85] applied a transparent photocatalytic coating containing TiO₂ particles on the architectural mortar; its photocatalytic performances was better than the TiO₂ intermixed samples on air purifying and self-cleaning properties under both UV-A and visible light irradiation conditions, and their abilities showed no obvious deterioration during a simulated facade-weathering process.

3.3. Paints

The commercial TiO₂, P25 (75% anatase and 25% rutile phases), is commonly applied in paints. Guo et al. [86] directly applied a TiO₂-containing paint (clear in colour) on the surface of self-compacting architectural mortars (SCAM). The results showed that the TiO₂ paint-coated SCAM sample displayed both a high photocatalytic rhodamine b removal ability and a robust weathering resistance under all conditions. Baudys et al. [87] investigated the photocatalytic properties of self-cleaning acrylic paint containing TiO₂ and ZnO using Acid Orange 7 as a model compound. The photocatalytic activity of TiO₂ increases with the weathering time. However, even if the initial photoactivity of the unweathered paints with ZnO was significantly higher, the photocatalytic activity decreased after weathering, due to the loss and/or photocorrosion of ZnO particles during the weathering process. Amorim et al. [88] synthesized an efficient and durable self-cleaning acrylic paint containing mesoporous TiO₂ (MTiO₂). The paint with MTiO₂ incorporated showed a better photoactivity and higher durability than the reference paint with P25 added in the cyclic analysis, which indicated that MTiO₂ microspheres can provide acrylic paint films with self-cleaning properties without severe degradation of the binder.

The self-cleaning photocatalytic paints could be designed for specific applications for outdoor or indoor environments. Most of these photocatalytic paints are based on titanium dioxide, however, the large band gap of TiO₂ requires UV photons for the electrons-holes generation, which makes it difficult to be efficient in the indoor environment. Galenda et al. [89] firstly compared the photocatalytic activity tests of indoor commercial self-cleaning paints under actual indoor light. These paints contain titanium dioxide with different amounts and crystallographic forms. The results of experiments with different lights suggest that all samples are scarcely active under visible light and the pollutant probes are selectively bleached due to their sensitizing effect. Consequently, the pollutants' ability in injecting electrons in the TiO₂ conduction band deeply affects their removal.

Paolini [90] propose a pre-treatment with nitric or sulfuric acid of commercial TiO₂ nanopowders to prevent from aging used in coating, mortars, or paints. photocatalytic performances for experiments with various diffuse reflectance of nitric and sulfuric acid were compared. Nitric acid causes a decrease in crystallinity and photocatalytic activity, which drops by almost 20%; and sulfuric acid is the best candidate for TiO₂ nanoparticles acid treatment with the aim of improving both their reflectance in a wavelength region unaffected by aging and sustaining their photocatalytic activity over time.

3.4. Construction Materials

Diamanti et al. [91] investigated the photocatalytic and self-cleaning activity of colored mortars containing TiO₂, and its possible interaction with iron oxide pigments, which are commonly added to the mixture in the production of colored mortars. Because of the self-cleaning characteristics, TiO₂ containing mortars have lower soiling in atmospheric exposure. However, the Iron oxide pigments caused lower photocatalytic activity compared to white mortars. Nath et al. [92] reviewed the photocatalysts used in concrete and found that majority of the work in concrete adopted TiO₂ as the photocatalyst. They also regarded the semiconductor oxide LiNbO₃, which has been used in electronic instruments to replace TiO₂ for artificial photosynthesis, as a promising and relatively new approach to be used in future concrete.

For the applications of photocatalysts on buildings, it is clear that the photocatalyst TiO₂ dominates the application market, and very few applications adopt other catalysts such as ZnO. Due to its low cost, high chemical stability and non-toxic properties, TiO₂ has been investigated extensively and first applied to the practical applications on buildings. Since various materials have different properties, other materials will also be applied in the near future according to their characteristics.

4. Conclusions

Thermal catalytic and photocatalytic nanomaterials are increasingly being used as an efficient approach to remove the VOCs, and their emerging applications on building and construction materials

are promising for their air-cleaning properties. Among these catalysts, TiO₂ is the most common, economical and efficient one due to its low cost, high chemical stability, and non-toxic properties. TiO₂ has been investigated for decades and dominates the applications of catalytic VOC removal on buildings. Since other thermal catalysts also showed brilliant performance and have been studied continuously, there is expected to be more applications on buildings using other emerging catalysts rather than TiO₂. As the photocatalysis performances of metal oxides can be enhanced by the synergy with hybrid adsorption materials [6], more catalysts combining different nanomaterials are expected. Among various applications of catalytic nanomaterials on buildings, the approach of coatings is more efficient and prevalent compared to intermixing [85] on the removal of VOCs. In order to remove the indoor VOCs more efficiently, more researches and applications should be done to increase their efficiencies in specific conditions such as visible light.

Author Contributions: Review proposal, K.W.S.; Information collection, K.W.S. and W.L.; Developing structure, K.W.S. and W.L.; Supervision, K.W.S.; Writing—Original Draft, W.L.; Writing—Review & Editing, K.W.S.

Funding: This research was funded by National Research Foundation (Singapore) grant number NRF2015NRF-POC001-0025 and National University of Singapore grant R-296-000-174-720.

Acknowledgments: Acknowledgement is given to Department of Building, National University of Singapore.

Conflicts of Interest: The authors declare no conflict of interest.

References

1. Spengler, J.D.; Chen, Q. Indoor air quality factors in designing a healthy building. *Annu. Rev. Energy Environ.* **2000**, *25*, 567–600. [[CrossRef](#)]
2. Jones, A.P. Indoor air quality and health. *Atmos. Environ.* **1999**, *33*, 4535–4564. [[CrossRef](#)]
3. Maroni, M.; Seifert, B.; Lindvall, T. *Indoor Air Quality: A Comprehensive Reference Book*; Elsevier: New York, NY, USA, 1995; Volume 3.
4. Weschler, C.J. Ozone's impact on public health: Contributions from indoor exposures to ozone and products of ozone-initiated chemistry. *Environ. Health Perspect.* **2006**, *114*, 1489–1496. [[CrossRef](#)] [[PubMed](#)]
5. Yang, C.; Miao, G.; Pi, Y.; Xia, Q.; Wu, J.; Li, Z.; Xiao, J. Abatement of various types of VOCs by adsorption/catalytic oxidation: A review. *Chem. Eng. J.* **2019**, *370*, 1128–1153. [[CrossRef](#)]
6. Li, M.; Lu, B.; Ke, Q.-F.; Guo, Y.-J.; Guo, Y.-P. Synergetic effect between adsorption and photodegradation on nanostructured TiO₂/activated carbon fiber felt porous composites for toluene removal. *J. Hazard. Mater.* **2017**, *333*, 88–98. [[CrossRef](#)] [[PubMed](#)]
7. González-García, P. Activated carbon from lignocellulosics precursors: A review of the synthesis methods, characterization techniques and applications. *Renew. Sustain. Energy Rev.* **2018**, *82*, 1393–1414. [[CrossRef](#)]
8. Spokas, K.A.; Novak, J.M.; Stewart, C.E.; Cantrell, K.B.; Uchimiyu, M.; DuSaire, M.G.; Ro, K.S. Qualitative analysis of volatile organic compounds on biochar. *Chemosphere* **2011**, *85*, 869–882. [[CrossRef](#)]
9. Zhang, X.; Gao, B.; Creamer, A.E.; Cao, C.; Li, Y. Adsorption of VOCs onto engineered carbon materials: A review. *J. Hazard. Mater.* **2017**, *338*, 102–123. [[CrossRef](#)]
10. Zhang, Z.; Chen, J.; Gao, Y.; Ao, Z.; Li, G.; An, T.; Hu, Y.; Li, Y. A coupled technique to eliminate overall nonpolar and polar volatile organic compounds from paint production industry. *J. Clean. Prod.* **2018**, *185*, 266–274. [[CrossRef](#)]
11. Tompkins, D.T.; Anderson, M.A. *Evaluation of Photocatalytic Air Cleaning Capability: A Literature Review & Engineering Analysis*; ASHRAE: Atlanta, GA, USA, 2001.
12. Mo, J.; Zhang, Y.; Xu, Q.; Lamson, J.J.; Zhao, R. Photocatalytic purification of volatile organic compounds in indoor air: A literature review. *Atmos. Environ.* **2009**, *43*, 2229–2246. [[CrossRef](#)]
13. Chen, H.; Nanayakkara, C.E.; Grassian, V.H. Titanium Dioxide Photocatalysis in Atmospheric Chemistry. *Chem. Rev.* **2012**, *112*, 5919–5948. [[CrossRef](#)] [[PubMed](#)]
14. Shayegan, Z.; Lee, C.-S.; Haghigat, F. TiO₂ photocatalyst for removal of volatile organic compounds in gas phase—A review. *Chem. Eng. J.* **2018**, *334*, 2408–2439. [[CrossRef](#)]
15. Cheng, M.; Brown, S. VOCs Identified in Australian Indoor Air and Product Emission Environments. In Proceedings of the National Clean Air Conference, Beijing, China, 4–9 September 2005; pp. 23–27.

16. Wang, S.; Ang, H.M.; Tade, M.O. Volatile organic compounds in indoor environment and photocatalytic oxidation: State of the art. *Environ. Int.* **2007**, *33*, 694–705. [[CrossRef](#)] [[PubMed](#)]
17. Kang, D.H.; Choi, D.H.; Lee, S.M.; Yeo, M.S.; Kim, K.W. Effect of bake-out on reducing VOC emissions and concentrations in a residential housing unit with a radiant floor heating system. *Build. Environ.* **2010**, *45*, 1816–1825. [[CrossRef](#)]
18. Kim, S.; Choi, Y.-K.; Park, K.-W.; Kim, J.T. Test methods and reduction of organic pollutant compound emissions from wood-based building and furniture materials. *Bioresour. Technol.* **2010**, *101*, 6562–6568. [[CrossRef](#)] [[PubMed](#)]
19. Zheng, L.; Shah, K.W. Chapter 16: Electrochromic Smart Windows for Green Building Applications. In *RSC Smart Materials*; Royal Society of Chemistry: London, UK, 2019; pp. 494–520.
20. Huseien, G.F.; Sam, A.R.M.; Shah, K.W.; Asaad, M.A.; Tahir, M.M.; Mirza, J. Properties of ceramic tile waste based alkali-activated mortars incorporating GBFS and fly ash. *Constr. Build. Mater.* **2019**, *214*, 355–368. [[CrossRef](#)]
21. Seh, Z.W.; Liu, S.; Zhang, S.Y.; Shah, K.W.; Han, M.Y. Synthesis and multiple reuse of eccentric Au@TiO₂ nanostructures as catalysts. *Chem. Commun.* **2011**, *47*, 6689–6691. [[CrossRef](#)]
22. Hussain, M.; Akhter, P.; Iqbal, J.; Ali, Z.; Yang, W.; Shehzad, N.; Majeed, K.; Sheikh, R.; Amjad, U.; Russo, N. VOCs photocatalytic abatement using nanostructured titania-silica catalysts. *J. Environ. Chem. Eng.* **2017**, *5*, 3100–3107. [[CrossRef](#)]
23. Singh, E.; Meyyappan, M.; Nalwa, H.S. Flexible Graphene-Based Wearable Gas and Chemical Sensors. *ACS Appl. Mater. Interfaces* **2017**, *9*, 34544–34586. [[CrossRef](#)]
24. Andre, R.S.; Sanfelice, R.C.; Pavinatto, A.; Mattoso, L.H.C.; Correa, D.S. Hybrid nanomaterials designed for volatile organic compounds sensors: A review. *Mater. Des.* **2018**, *156*, 154–166. [[CrossRef](#)]
25. Kwon, S.; Fan, M.; Cooper, A.T.; Yang, H. Photocatalytic applications of micro- and nano-TiO₂ in environmental engineering. *Crit. Rev. Environ. Sci. Technol.* **2008**, *38*, 197–226. [[CrossRef](#)]
26. Tsang, C.H.A.; Li, K.; Zeng, Y.; Zhao, W.; Zhang, T.; Zhan, Y.; Xie, R.; Leung, D.Y.C.; Huang, H. Titanium oxide based photocatalytic materials development and their role of in the air pollutants degradation: Overview and forecast. *Environ. Int.* **2019**, *125*, 200–228. [[CrossRef](#)]
27. Hu, M.; Yao, Z.; Wang, X. Graphene-based nanomaterials for catalysis. *Ind. Eng. Chem. Res.* **2017**, *56*, 3477–3502. [[CrossRef](#)]
28. Pan, Y.; Yuan, X.; Jiang, L.; Yu, H.; Zhang, J.; Wang, H.; Guan, R.; Zeng, G. Recent advances in synthesis, modification and photocatalytic applications of micro/nano-structured zinc indium sulfide. *Chem. Eng. J.* **2018**, *354*, 407–431. [[CrossRef](#)]
29. Sharma, R.; Sharma, S.; Dutta, S.; Zboril, R.; Gawande, M.B. Silica-nanosphere-based organic-inorganic hybrid nanomaterials: Synthesis, functionalization and applications in catalysis. *Gr. Chem.* **2015**, *17*, 3207–3230. [[CrossRef](#)]
30. Huang, H.; Xu, Y.; Feng, Q.; Leung, D.Y. Low temperature catalytic oxidation of volatile organic compounds: A review. *Catal. Sci. Technol.* **2015**, *5*, 2649–2669. [[CrossRef](#)]
31. Pelaez, M.; Nolan, N.T.; Pillai, S.C.; Seery, M.K.; Falaras, P.; Kontos, A.G.; Dunlop, P.S.M.; Hamilton, J.W.J.; Byrne, J.A.; O’Shea, K.; et al. A review on the visible light active titanium dioxide photocatalysts for environmental applications. *Appl. Catal. B Environ.* **2012**, *125*, 331–349. [[CrossRef](#)]
32. Truppi, A.; Petronella, F.; Placido, T.; Striccoli, M.; Agostiano, A.; Curri, M.; Comparelli, R. Visible-light-active TiO₂-based hybrid nanocatalysts for environmental applications. *Catalysts* **2017**, *7*, 100. [[CrossRef](#)]
33. Maira, A.J.; Yeung, K.L.; Lee, C.Y.; Yue, P.L.; Chan, C.K. Size Effects in Gas-Phase Photo-oxidation of Trichloroethylene Using Nanometer-Sized TiO₂ Catalysts. *J. Catal.* **2000**, *192*, 185–196. [[CrossRef](#)]
34. Maira, A.J.; Coronado, J.M.; Augugliaro, V.; Yeung, K.L.; Conesa, J.C.; Soria, J. Fourier Transform Infrared Study of the Performance of Nanostructured TiO₂ Particles for the Photocatalytic Oxidation of Gaseous Toluene. *J. Catal.* **2001**, *202*, 413–420. [[CrossRef](#)]
35. Lee, H.J.; Seo, H.O.; Kim, D.W.; Kim, K.-D.; Luo, Y.; Lim, D.C.; Ju, H.; Kim, J.W.; Lee, J.; Kim, Y.D. A high-performing nanostructured TiO₂ filter for volatile organic compounds using atomic layer deposition. *Chem. Commun.* **2011**, *47*, 5605–5607. [[CrossRef](#)] [[PubMed](#)]
36. Weon, S.; Choi, W. TiO₂ Nanotubes with Open Channels as Deactivation-Resistant Photocatalyst for the Degradation of Volatile Organic Compounds. *Environ. Sci. Technol.* **2016**, *50*, 2556–2563. [[CrossRef](#)] [[PubMed](#)]

37. Weon, S.; Choi, J.; Park, T.; Choi, W. Freestanding doubly open-ended TiO₂ nanotubes for efficient photocatalytic degradation of volatile organic compounds. *Appl. Catal. B Environ.* **2017**, *205*, 386–392. [[CrossRef](#)]
38. Wu, C.; Yue, Y.; Deng, X.; Hua, W.; Gao, Z. Investigation on the synergetic effect between anatase and rutile nanoparticles in gas-phase photocatalytic oxidations. *Catal. Today* **2004**, *93–95*, 863–869. [[CrossRef](#)]
39. Chen, K.; Zhu, L.; Yang, K. Tricrystalline TiO₂ with enhanced photocatalytic activity and durability for removing volatile organic compounds from indoor air. *J. Environ. Sci.* **2015**, *32*, 189–195. [[CrossRef](#)] [[PubMed](#)]
40. Zhong, L.; Brancho, J.J.; Batterman, S.; Bartlett, B.M.; Godwin, C. Experimental and modeling study of visible light responsive photocatalytic oxidation (PCO) materials for toluene degradation. *Appl. Catal. B Environ.* **2017**, *216*, 122–132. [[CrossRef](#)]
41. Qiu, X.; Miyachi, M.; Sunada, K.; Minoshima, M.; Liu, M.; Lu, Y.; Li, D.; Shimodaira, Y.; Hosogi, Y.; Kuroda, Y.; et al. Hybrid Cu_xO/TiO₂ nanocomposites as risk-reduction materials in indoor environments. *ACS Nano* **2012**, *6*, 1609–1618. [[CrossRef](#)] [[PubMed](#)]
42. Weon, S.; Kim, J.; Choi, W. Dual-components modified TiO₂ with Pt and fluoride as deactivation-resistant photocatalyst for the degradation of volatile organic compound. *Appl. Catal. B Environ.* **2018**, *220*, 1–8. [[CrossRef](#)]
43. Li, J.J.; Cai, S.C.; Yu, E.Q.; Weng, B.; Chen, X.; Chen, J.; Jia, H.P.; Xu, Y.J. Efficient infrared light promoted degradation of volatile organic compounds over photo-thermal responsive Pt-rGO-TiO₂ composites. *Appl. Catal. B Environ.* **2018**, *233*, 260–271. [[CrossRef](#)]
44. Suárez, S.; Jansson, I.; Ohtani, B.; Sánchez, B. From titania nanoparticles to decahedral anatase particles: Photocatalytic activity of TiO₂/zeolite hybrids for VOCs oxidation. *Catal. Today* **2019**, *326*, 2–7. [[CrossRef](#)]
45. Li, X.; Zhu, Z.; Zhao, Q.; Wang, L. Photocatalytic degradation of gaseous toluene over ZnAl₂O₄ prepared by different methods: A comparative study. *J. Hazard. Mater.* **2011**, *186*, 2089–2096. [[CrossRef](#)]
46. Jiang, S.; Handberg, E.S.; Liu, F.; Liao, Y.; Wang, H.; Li, Z.; Song, S. Effect of doping the nitrogen into carbon nanotubes on the activity of NiO catalysts for the oxidation removal of toluene. *Applied Catal. B Environ.* **2014**, *160–161*, 716–721. [[CrossRef](#)]
47. Kim, H.I.; Kim, H.N.; Weon, S.; Moon, G.H.; Kim, J.H.; Choi, W. Robust Co-catalytic performance of nanodiamonds loaded on WO₃ for the decomposition of volatile organic compounds under visible light. *ACS Catal.* **2016**, *6*. [[CrossRef](#)]
48. Genuino, H.C.; Dharmarathna, S.; Njagi, E.C.; Mei, M.C.; Suib, S.L. Gas-phase total oxidation of benzene, toluene, ethylbenzene, and xylenes using shape-selective manganese oxide and copper manganese oxide catalysts. *J. Phys. Chem. C* **2012**, *116*, 12066–12078. [[CrossRef](#)]
49. Miyawaki, J.; Lee, G.H.; Yeh, J.; Shiratori, N.; Shimohara, T.; Mochida, I.; Yoon, S.H. Development of carbon-supported hybrid catalyst for clean removal of formaldehyde indoors. *Catal. Today* **2012**, *185*, 278–283. [[CrossRef](#)]
50. Qian, X.; Yue, D.; Tian, Z.; Reng, M.; Zhu, Y.; Kan, M.; Zhang, T.; Zhao, Y. Carbon quantum dots decorated Bi₂WO₆ nanocomposite with enhanced photocatalytic oxidation activity for VOCs. *Appl. Catal. B Environ.* **2016**, *193*, 16–21. [[CrossRef](#)]
51. Cao, J.; Luo, B.; Lin, H.; Chen, S. Photocatalytic activity of novel AgBr/WO₃ composite photocatalyst under visible light irradiation for methyl orange degradation. *J. Hazard. Mater.* **2011**, *190*, 700–706. [[CrossRef](#)]
52. Abbasi, Z.; Haghghi, M.; Fatehifar, E.; Saedy, S. Synthesis and physicochemical characterizations of nanostructured Pt/Al₂O₃-CeO₂ catalysts for total oxidation of VOCs. *J. Hazard. Mater.* **2011**, *186*, 1445–1454. [[CrossRef](#)]
53. Chen, Z.; Mao, J.; Zhou, R. Preparation of size-controlled Pt supported on Al₂O₃ nanocatalysts for deep catalytic oxidation of benzene at lower temperature. *Appl. Surf. Sci.* **2019**, *465*, 15–22. [[CrossRef](#)]
54. Wang, L.; Sakurai, M.; Kameyama, H. Study of catalytic decomposition of formaldehyde on Pt/TiO₂ alumite catalyst at ambient temperature. *J. Hazard. Mater.* **2009**, *167*, 399–405. [[CrossRef](#)]
55. Schick, L.; Sanchis, R.; González-Alfaro, V.; Agouram, S.; López, J.M.; Torrente-Murciano, L.; García, T.; Solsona, B. Size-activity relationship of iridium particles supported on silica for the total oxidation of volatile organic compounds (VOCs). *Chem. Eng. J.* **2019**, *366*, 100–111. [[CrossRef](#)]
56. Joung, H.-J.; Kim, J.-H.; Oh, J.-S.; You, D.-W.; Park, H.-O.; Jung, K.-W. Catalytic oxidation of VOCs over CNT-supported platinum nanoparticles. *Appl. Surf. Sci.* **2014**, *290*, 267–273. [[CrossRef](#)]

57. Zhang, Y.; Tang, Z.-R.; Fu, X.; Xu, Y.-J. TiO₂–Graphene Nanocomposites for Gas-Phase Photocatalytic Degradation of Volatile Aromatic Pollutant: Is TiO₂–Graphene Truly Different from Other TiO₂–Carbon Composite Materials? *ACS Nano* **2010**, *4*, 7303–7314. [[CrossRef](#)]
58. Roso, M.; Boaretti, C.; Pelizzo, M.G.; Lauria, A.; Modesti, M.; Lorenzetti, A. Nanostructured Photocatalysts Based on Different Oxidized Graphenes for VOCs Removal. *Ind. Eng. Chem. Resour.* **2017**, *56*, 9980–9992. [[CrossRef](#)]
59. Demeestere, K.; Dewulf, J.; Van Langenhove, H. Heterogeneous Photocatalysis as an Advanced Oxidation Process for the Abatement of Chlorinated, Monocyclic Aromatic and Sulfurous Volatile Organic Compounds in Air: State of the Art. *Crit. Rev Environ. Sci. Technol.* **2007**, *37*, 489–538. [[CrossRef](#)]
60. Fujishima, A.; Honda, K. Electrochemical Photolysis of Water at a Semiconductor Electrode. *Nature* **1972**, *238*, 37–38. [[CrossRef](#)] [[PubMed](#)]
61. Di Paola, A.; Bellardita, M.; Palmisano, L. Brookite, the least known TiO₂ photocatalyst. *Catalysts* **2013**, *3*, 36–73. [[CrossRef](#)]
62. Monai, M.; Montini, T.; Fornasiero, P. Brookite: Nothing New under the Sun? *Catalysts* **2017**, *7*, 304. [[CrossRef](#)]
63. Jo, W.-K.; Kim, J.-T. Application of visible-light photocatalysis with nitrogen-doped or unmodified titanium dioxide for control of indoor-level volatile organic compounds. *J. Hazard. Mater.* **2009**, *164*, 360–366. [[CrossRef](#)]
64. Elfalleh, W.; Assadi, A.A.; Bouzaza, A.; Wolbert, D.; Kiwi, J.; Rtimi, S. Innovative and stable TiO₂ supported catalytic surfaces removing aldehydes under UV-light irradiation. *J. Photochem. Photobiol. A Chem.* **2017**, *343*, 96–102. [[CrossRef](#)]
65. Assadi, A.A.; Bouzaza, A.; Wolbert, D.; Petit, P. Isovaleraldehyde elimination by UV/TiO₂ photocatalysis: Comparative study of the process at different reactors configurations and scales. *Environ. Sci. Pollut. Res.* **2014**, *21*, 11178–11188. [[CrossRef](#)] [[PubMed](#)]
66. Palau, J.; Assadi, A.A.; Penya-Roja, J.; Bouzaza, A.; Wolbert, D.; Martínez-Soria, V. Isovaleraldehyde degradation using UV photocatalytic and dielectric barrier discharge reactors, and their combinations. *J. Photochem. Photobiol. A Chemis.* **2015**, *299*, 110–117. [[CrossRef](#)]
67. Azzouz, I.; Habba, Y.G.; Capochichi-Gnambodoe, M.; Marty, F.; Vial, J.; Leprince-Wang, Y.; Bourouina, T. Zinc oxide nano-enabled microfluidic reactor for water purification and its applicability to volatile organic compounds. *Microsyst. Nanoengin.* **2018**, *4*. [[CrossRef](#)]
68. Chen, J.; Chen, X.; Yan, D.; Jiang, M.; Xu, W.; Yu, H.; Jia, H. A facile strategy of enhancing interaction between cerium and manganese oxides for catalytic removal of gaseous organic contaminants. *Appl. Catal. B Environ.* **2019**, *250*, 396–407. [[CrossRef](#)]
69. Zhao, Q.; Liu, Q.; Song, C.; Ji, N.; Ma, D.; Lu, X. Enhanced catalytic performance for VOCs oxidation on the CoAlO oxides by KMnO₄ doped on facile synthesis. *Chemosphere* **2019**, *218*, 895–906. [[CrossRef](#)] [[PubMed](#)]
70. Kobayashi, B.; Yamamoto, R.; Ohkita, H.; Mizushima, T.; Hiraishi, A.; Kakuta, N. Photocatalytic Activity of AgBr as an Environmental Catalyst. *Top Catal.* **2013**, *56*, 618–622. [[CrossRef](#)]
71. Samaddar, P.; Son, Y.-S.; Tsang, D.C.W.; Kim, K.-H.; Kumard, S. Progress in graphene-based materials as superior media for sensing, sorption, and separation of gaseous pollutants. *Coord. Chem. Rev.* **2018**, *368*, 93–114. [[CrossRef](#)]
72. Munafò, P.; Quagliarini, E.; Goffredo, G.B.; Bondioli, F.; Licciulli, A. Durability of nano-engineered TiO₂ self-cleaning treatments on limestone. *Constr. Build. Mater.* **2014**, *65*, 218–231. [[CrossRef](#)]
73. Toro, C.; Jobson, B.T.; Haselbach, L.; Shen, S.; Chung, S.H. Photoactive roadways: Determination of CO, NO and VOC uptake coefficients and photolabile side product yields on TiO₂ treated asphalt and concrete. *Atmos. Environ.* **2016**, *139*, 37–45. [[CrossRef](#)]
74. Huseien, G.F.; Shah, K.W.; Sam, A.R.M. Sustainability of nanomaterials based self-healing concrete: An all-inclusive insight. *J. Build. Eng.* **2019**, *23*, 155–171. [[CrossRef](#)]
75. Li, L.; Zhang, F.; Zhong, Z.; Zhu, M.; Jiang, C.; Hu, J.; Xing, W. Novel Synthesis of a High-Performance Pt/ZnO/SiC Filter for the Oxidation of Toluene. *Ind. Eng. Chem. Res.* **2017**, *56*, 13857–13865. [[CrossRef](#)]
76. Zadi, T.; Assadi, A.A.; Nasrallah, N.; Bouallouche, R.; Tri, P.N.; Bouzaza, A.; Azizi, M.M.; Maachi, R.; Wolbert, D. Treatment of hospital indoor air by a hybrid system of combined plasma with photocatalysis: Case of trichloromethane. *Chem. Eng. J.* **2018**, *349*, 276–286. [[CrossRef](#)]
77. Li, F.B.; Li, X.Z.; Ao, C.H.; Lee, S.C.; Hou, M.F. Enhanced photocatalytic degradation of VOCs using Ln³⁺–TiO₂ catalysts for indoor air purification. *Chemosphere* **2005**, *59*, 787–800. [[CrossRef](#)] [[PubMed](#)]

78. Boyjoo, Y.; Sun, H.; Liu, J.; Pareek, V.K.; Wang, S. A review on photocatalysis for air treatment: From catalyst development to reactor design. *Chem. Eng. J.* **2017**, *310*, 537–559. [[CrossRef](#)]
79. Chabas, A.; Lombardo, T.; Cachier, H.; Pertuisot, M.H.; Oikonomou, K.; Falcone, R.; Verità, M.; Geotti-Bianchini, F. Behaviour of self-cleaning glass in urban atmosphere. *Build. Environ.* **2008**, *43*, 2124–2131. [[CrossRef](#)]
80. Oladipo, H.; Garlisi, C.; Al-Ali, K.; Azar, E.; Palmisano, G. Combined photocatalytic properties and energy efficiency via multifunctional glass. *J. Environ. Chem. Eng.* **2019**, *7*. [[CrossRef](#)]
81. Monteiro, R.A.R.; Lopes, F.V.S.; Silva, A.M.T.; Ângelo, J.; Silva, G.V.; Mendes, A.M.; Boaventura, R.A.R.; Vilar, V.J.P. Are TiO₂-based exterior paints useful catalysts for gas-phase photooxidation processes? A case study on n-decane abatement for air detoxification. *Appl. Catal. B Environ.* **2014**, *147*, 988–999. [[CrossRef](#)]
82. Martinez, T.; Bertron, A.; Escadeillas, G.; Ringot, E.; Simon, V. BTEX abatement by photocatalytic TiO₂-bearing coatings applied to cement mortars. *Build. Environ.* **2014**, *71*, 186–192. [[CrossRef](#)]
83. Zhong, L.; Haghghat, F.; Lee, C.S.; Lakdawala, N. Performance of ultraviolet photocatalytic oxidation for indoor air applications: Systematic experimental evaluation. *J. Hazard. Mater.* **2013**, *261*, 130–138. [[CrossRef](#)]
84. Jiang, Q.; Qi, T.; Yang, T.; Liu, Y. Ceramic tiles for photocatalytic removal of NO in indoor and outdoor air under visible light. *Build. Environ.* **2019**, *158*, 94–103. [[CrossRef](#)]
85. Guo, M.-Z.; Maury-Ramirez, A.; Poon, C.S. Photocatalytic activities of titanium dioxide incorporated architectural mortars: Effects of weathering and activation light. *Build. Environ.* **2015**, *94*, 395–402. [[CrossRef](#)]
86. Guo, M.-Z.; Maury-Ramirez, A.; Poon, C.S. Self-cleaning ability of titanium dioxide clear paint coated architectural mortar and its potential in field application. *J. Clean. Product.* **2016**, *112*, 3583–3588. [[CrossRef](#)]
87. Baudys, M.; Krýsa, J.; Zlámál, M.; Mills, A. Weathering tests of photocatalytic facade paints containing ZnO and TiO₂. *Chem. Eng. J.* **2015**, *261*, 83–87. [[CrossRef](#)]
88. Amorim, S.M.; Suave, J.; Andrade, L.; Mendes, A.M.; José, H.J.; Moreira, R.F.P.M. Towards an efficient and durable self-cleaning acrylic paint containing mesoporous TiO₂ microspheres. *Prog. Org. Coat.* **2018**, *118*, 48–56. [[CrossRef](#)]
89. Galenda, A.; Visentin, F.; Gerbasi, R.; Favaro, M.; Bernardi, A.; El Habra, N. Evaluation of self-cleaning photocatalytic paints: Are they effective under actual indoor lighting systems? *Appl. Catal. B Environ.* **2018**, *232*, 194–204. [[CrossRef](#)]
90. Paolini, R.; Borroni, D.; Pedefferri, M.; Diamanti, M.V. Self-cleaning building materials: The multifaceted effects of titanium dioxide. *Constr. Build. Mater.* **2018**, *182*, 126–133. [[CrossRef](#)]
91. Diamanti, M.V.; Del Curto, B.; Ormellese, M.; Pedefferri, M. Photocatalytic and self-cleaning activity of colored mortars containing TiO₂. *Constr. Build. Mater.* **2013**, *46*, 167–174. [[CrossRef](#)]
92. Nath, R.K.; Zain, M.F.M.; Jamil, M. An environment-friendly solution for indoor air purification by using renewable photocatalysts in concrete: A review. *Renew. Sustain. Energy Rev.* **2016**, *62*, 1184–1194. [[CrossRef](#)]

